Biophysical Journal
Article

Biophysical Society

Disentangling Viral Membrane Fusion from Receptor Binding Using Synthetic DNA-Lipid Conjugates

Robert J. Rawle,[1,2] Steven G. Boxer,[2] and Peter M. Kasson[1,*]
[1]Department of Molecular Physiology and Biological Physics, University of Virginia, Charlottesville, Virginia; and [2]Department of Chemistry, Stanford University, Stanford, California

ABSTRACT Enveloped viruses must bind to a receptor on the host membrane to initiate infection. Membrane fusion is subsequently initiated by a conformational change in the viral fusion protein, triggered by receptor binding, an environmental change, or both. Here, we present a strategy to disentangle the two processes of receptor binding and fusion using synthetic DNA-lipid conjugates to bind enveloped viruses to target membranes in the absence of receptor. This permits direct testing of whether receptor engagement affects the fusion mechanism as well as a comparison of fusion behavior across viruses with different receptor binding specificities. We demonstrate this approach by binding X-31 influenza virus to target vesicles and measuring the rates of individual pH-triggered lipid mixing events using fluorescence microscopy. Influenza lipid mixing kinetics are found to be independent of receptor binding, supporting the common yet previously unproven assumption that receptor binding does not produce any clustering or spatial rearrangement of viral hemagglutinin, which affects the rate-limiting step of pH-triggered fusion. This DNA-lipid tethering strategy should also allow the study of viruses where challenging receptor reconstitution has previously prevented single-virus fusion experiments.

INTRODUCTION

Before entering a host cell to initiate infection, enveloped viruses must first bind to receptor(s) on the host plasma membrane, often glycolipids or glycoproteins. For viruses such as human immunodeficiency virus, (co-)receptor binding triggers a conformational change in the viral fusion protein that permits the fusion of viral and host membranes, initiating virus entry (1–3). For viruses such as influenza, receptor binding is followed by endocytosis, and viral fusion is triggered by the pH drop that accompanies endosomal maturation (1,4). For other viruses, the fusion trigger may involve both receptor binding and an environmental change (5,6). Membrane fusion has been studied extensively for many viruses, but key biophysical questions remain unanswered, precisely because fusion involves dynamic interactions between proteins and lipids on both viral and host membranes.

Recently, fusion experiments between single virus particles and artificial lipid membranes have been employed to address some of these biophysical questions (7–12). In these experiments, isolated host receptors were incorporated into artificial target membranes assembled on solid supports. Receptor binding and membrane fusion (typically lipid mixing) of individual fluorescently labeled virus particles were studied by fluorescence microscopy. The waiting time distributions compiled from many individual virus fusion events were then fit to kinetic models and compared across different viral mutants and/or experimental conditions to extract biophysical mechanistic information. These single virus fusion experiments have produced promising insight into various aspects of the fusion process, such as more direct estimates of the number of viral fusion proteins involved and the role of different fusion intermediates. Additionally, only fusion of prebound viral particles is observed because all unbound viral particles are removed by rinsing before triggering fusion. Consequently, these measurements are able to cleanly separate receptor binding from subsequent fusion steps—a potentially confounding variable in the more conventional bulk fusion experiments. However, these experiments rely upon having an isolated host receptor in the target membrane, and so it becomes difficult to study the role of receptor binding on fusion, as well as to study viruses whose receptor(s) is unknown or difficult to reconstitute.

Herein, we present a general strategy to use synthetic DNA-lipid conjugates to tether enveloped virions to target

Submitted February 12, 2016, and accepted for publication May 25, 2016.
*Correspondence: kasson@virginia.edu
Editor: Claudia Steinem.
http://dx.doi.org/10.1016/j.bpj.2016.05.048

membranes in the absence of receptor. These DNA-lipids are short DNA oligomers covalently coupled to a double-tailed lipid by phosphoramidite chemistry and can be designed with variable length, sequence, and binding geometry (13). They insert spontaneously into model membranes, and hybridization between complementary DNA-lipids has previously been used to tether model membranes to each other or to solid supports and to mediate binding between cells (13–16). Binding specificity is programmed by the DNA sequence. In this work, we show that these DNA-lipids can also be used to tether enveloped virus particles to target membranes in the absence of the native receptor. We demonstrate that DNA-lipids can be incorporated into X-31 influenza virions and will tether virions to glass-supported bilayers containing complementary DNA-lipids in the absence of the native sialic acid receptors. We measure the distribution of DNA-lipids incorporated into influenza virions by single molecule and quantitative fluorescence imaging.

We then apply this DNA-lipid tethering strategy, together with a single virus lipid mixing assay, to study the role of receptor binding on influenza (hemi-)fusion kinetics. Influenza A virus is an enveloped, negative-sense RNA virus, which enters host cells by first binding to its receptor—a sialic acid-terminated glycan—on the host cell plasma membrane (4). This receptor is bound by the viral membrane protein hemagglutinin (HA), which exists as a trimer at a high density in the viral envelope (~300 HAs per 100 nm diameter virus, see (17)). Following receptor binding, the virus is internalized by endocytosis. During endosomal maturation, the pH inside the endosome decreases, and when it drops below a critical value (pH 5–6), HA is triggered to undergo a dramatic conformational rearrangement, inserting a hydrophobic fusion peptide into the endosomal membrane, and inducing membrane fusion. Previous work has suggested that several HA trimers must act together to efficiently facilitate this fusion process—both lipid mixing (hemifusion) and content transfer (full fusion) (7,8,18). However, it remains unknown whether receptor binding causes clustering or other spatial rearrangements of HA that influence the subsequent pH-triggered fusion mechanism. For instance, if receptor binding caused HA clustering, the virus could be primed for fusion, resulting in faster pH-triggered fusion kinetics. Alternatively, receptor binding could create steric hindrance in a manner that could slow the conformational rearrangement of HA following pH drop, resulting in slower pH-triggered fusion kinetics. It is often assumed that the pH-triggered fusion kinetics is independent of receptor binding, but in the absence of an approach to bind influenza to a target membrane without receptors, this assumption has previously remained unproven. Our DNA-lipid tethering approach provides an opportunity to test this hypothesis. Using a single virus lipid mixing assay, we examined the lipid mixing kinetics of X-31 influenza bound to target large unilamellar vesicles either by DNA-lipid or by native receptor (a sialic acid-terminated glycolipid, schematic; see Fig. 1). We observed that the waiting time distributions of individual lipid mixing events were identical regardless of whether the virus was bound by DNA-lipid or by native receptor. This suggests that receptor binding does not alter HA conformation or spatial distribution in a way that affects the rate-limiting step of the (hemi-) fusion mechanism.

We note that while we only apply our DNA-lipid tethering strategy to influenza A virus in the current report, we anticipate that this strategy should be transferable to other enveloped viruses and may be of particular interest for viruses whose receptor is unknown or difficult to isolate.

MATERIALS AND METHODS

Materials

Dioleoyl phosphatidylethanolamine, Palmitoyl oleoyl phosphatidylcholine (POPC), and cholesterol were purchased from Avanti Polar Lipids (Alabaster,

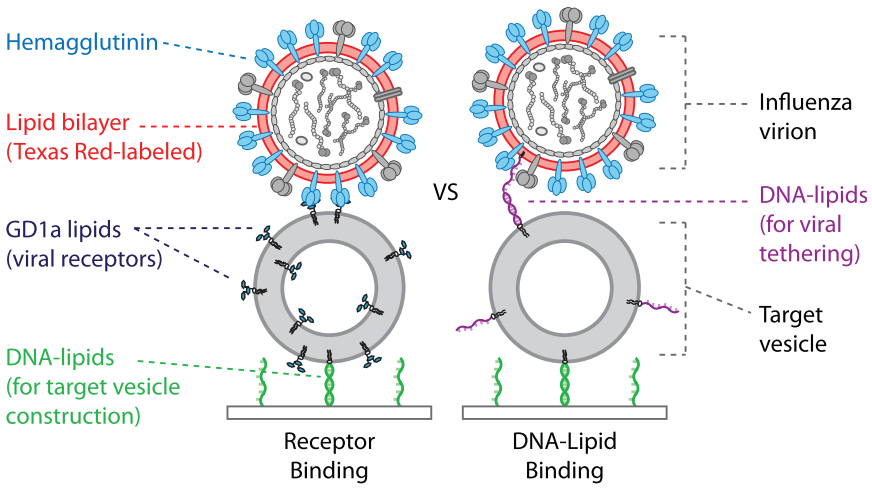

FIGURE 1 Schematic of influenza virions bound to target DNA-tethered lipid vesicles (*gray circles*) by (*left*) viral hemagglutinin (*light blue*) binding to glycolipid receptors (*black*) in the target vesicle or (*right*) hybridization of complementary DNA-lipids (*purple strands*) in virus and vesicle membranes. In both cases, target vesicles are tethered to the substrate by DNA-lipid hybridization (*green strands*, sequence orthogonal to *purple strands*) to the complementary DNA strand displayed on the substrate surface. Viral membranes are labeled with Texas Red (*red*). Nothing is drawn to scale. For reference, a labeled schematic of influenza virus components is shown in Fig. S1. To see this figure in color, go online.

AL). Texas Red-1,2-dihexadecanoyl-*sn*-glycero-3-phosphoethanolamine (TR-DHPE), Oregon Green-1,2-dihexadecanoyl-*sn*-glycero-3-phosphoethanolamine (OG-DHPE), and Alexa 546-succinimidyl ester were purchased from Thermo Fisher Scientific (Waltham, MA). Chloroform, methanol, and buffer salts were obtained from Fisher Scientific (Pittsburgh, PA) and Sigma-Aldrich (St. Louis, MO). Disialoganglioside GD1a from bovine brain (Cer-Glc-Gal(NeuAc)-GalNAc-Gal-NeuAc) was purchased from Sigma-Aldrich. 11-Azidoundecyltrimethoxysilane was obtained from Sikemia (Clapiers, France). Tridecafluoro-1,1,2,2-tetrahydrooctyltrichlorosilane was obtained from Gelest (Morrisville, PA). 1,1′,1″-tris(1H-1,2,3-triazol-4-yl-1-acetic acid ethyl ester) trimethylamine ligand was a generous gift from Professor Christopher Chidsey at Stanford University. Ethynyl phosphonic acid was synthesized as previously described (19).

Buffers

The following buffers were used. Vesicle Buffer = 10 mM NaH2PO4, 90 mM sodium citrate, 150 mM NaCl, pH 7.4. Fusion Buffer = 10 mM NaH2PO4, 90 mM sodium citrate, 150 mM NaCl, pH 5.0. HB buffer = 20 mM Hepes, 150 mM NaCl, pH 7.2.

Microscopy

All epifluorescence micrographs and videos were acquired with a Nikon Ti-U microscope using a 100× oil immersion objective, NA = 1.49 (Nikon Instruments, Melville, NY), with a Spectra-X LED Light Engine (Lumencor, Beaverton, OR) as an excitation light source, and additional excitation/emission filter wheels. Images were recorded with an Andor iXon 897 EMCCD camera (Andor Technologies, Belfast, UK) using 16-bit image settings, and were captured with Metamorph software (Molecular Devices, Sunnyvale, CA). Additional microscopy details are in the Supporting Materials and Methods in the Supporting Material.

DNA-lipid preparation and DNA sequences used

DNA-lipids were used to bind influenza virions to model lipid membranes in the absence of receptor and to construct DNA-tethered vesicles—the targets for lipid mixing experiments. DNA-lipid conjugation was achieved by phosphoramidite coupling and was purified by high-performance liquid chromatography, as previously described (13). Previous work has also demonstrated that these DNA-lipids insert spontaneously and quantitatively into lipid vesicles following an overnight incubation at 4°C (13). The sequences of DNA-lipids used in this study are listed in Table S1. Additional details about alkyne-DNA functionalization (used in the construction of the target DNA-tethered vesicles) and dye-DNA-lipid conjugation (used to determine the distribution of DNA-lipids incorporated into virions) are given in the Supporting Materials and Methods.

Single virus lipid mixing assay

Our single virus lipid mixing assay consisted of several components, each of which is described separately, and shown schematically, see Fig. 2. Additional details for each of these components are given below and in the Supporting Methods. 1) All measurements were made inside a microfluidic flow cell. 2) The glass coverslip inside the flow cell was functionalized with short DNA oligomers via alkyne-azide click chemistry to enable DNA-tethering of target vesicles. 3) Vesicles with DNA-lipids were then tethered to the modified coverslip by DNA hybridization, along with pH indicator membranes (not depicted, see Fig. 2). 4) Dye-labeled virions with DNA-lipids were bound to target vesicles. 5) Any unbound or loosely bound virus particles were removed by extensive rinsing of the flow cell. 6) Low pH buffer was infused, and single virus lipid mixing events were monitored by fluorescence microscopy.

Polydimethylsiloxane flow cells

All virus binding experiments, lipid mixing assays, and measurements of the DNA-lipid distribution in the viral particles were performed inside polydimethylsiloxane flow cells on glass coverslips. See Supporting Materials and Methods for details of flow cell design and preparation, as well as functionalization of the glass coverslip with DNA oligomers by click chemistry.

Vesicle preparation

Large unilamellar vesicles were prepared by extrusion with a nominal diameter of 100 nm using a lipid mixture of 67.5% POPC, 20% Dioleoyl phosphatidylethanolamine, 10% cholesterol, 2% GD1a, and 0.5% OG-DHPE (140 nmol total lipids). For vesicles prepared without GD1a, an additional 2% POPC was used instead. To incorporate DNA-lipids into vesicles, DNA-lipids were added to the suspension of vesicles, and incubated overnight at 4°C. See Supporting Materials and Methods for details.

DNA-tethered target vesicles and pH indicator membranes

DNA-tethered vesicles (schematics; see Figs. 1 and 2) were used as the target membranes in single virus lipid mixing experiments. To prepare

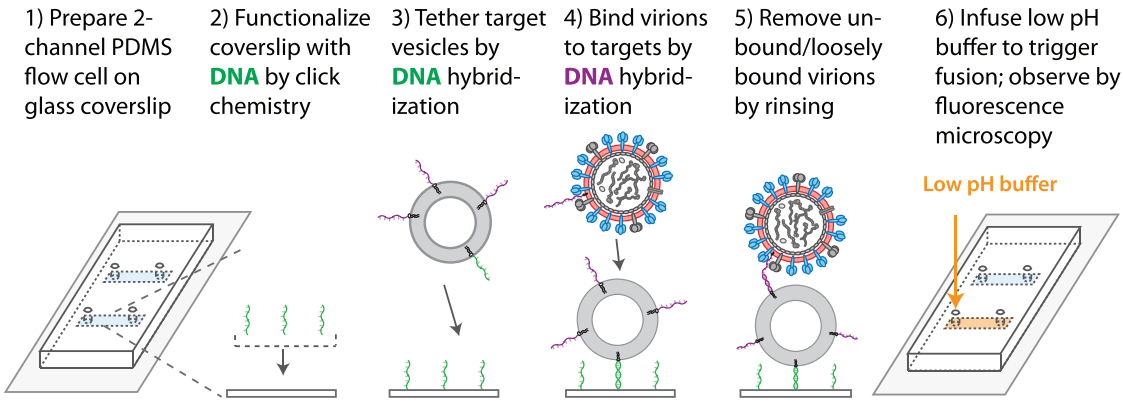

FIGURE 2 Schematic of preparation of single virus lipid mixing assay, details in Materials and Methods. Note that the virus is shown binding to the target vesicle by DNA hybridization (*purple strands*). In the case of GD1a receptor binding, these DNA-lipids would be replaced by GD1a glycolipids (as in the *left panel* in Fig. 1). To see this figure in color, go online.

DNA-tethered vesicles, DNA-lipids (sequence A, *green*; see Figs. 1 and 2) at 0.01 mol % were incorporated into vesicles. For experiments in which virus was bound to target vesicles via DNA-lipid hybridization, 0.03 mol % of sequence C DNA-lipids (*purple*; see Figs. 1 and 2) were also incorporated into the vesicles. Following DNA-lipid incorporation, vesicles displaying DNA were tethered inside a polydimethylsiloxane flow cell to a DNA-modified glass coverslip displaying the complementary DNA (sequence B; see Supporting Materials and Methods for preparation of DNA-modified glass coverslips). To achieve this, 15 μL of vesicles displaying DNA (0.56 mM nominal total lipid concentration) were mixed into the flow cell and incubated for at least 90 min. The flow cell was then rinsed with at least 3 mL of Vesicle Buffer. This resulted in a densely packed surface of DNA-tethered vesicles, where the separation distance between many adjacent tethered vesicles was near or below the diffraction limit, as observed by fluorescence microscopy. Because of the small surface area available for binding on these target tethered vesicles (~100 nm diameter), this high density of tethered vesicles was necessary to ensure that enough viral particles would bind to the target vesicles during a reasonable experimental timescale while minimizing the amount of virus consumed in each experiment.

To accurately determine the time of pH drop at the sample surface during lipid mixing experiments, a low density of OG-DHPE pH indicator membranes was also prepared inside the flow cell. Oregon Green is pH sensitive across the pH range of our experiments. These pH indicator membranes were DNA-tethered membrane patches formed from giant unilamellar vesicles, whose construction we have described previously in other contexts (15,20). See Supporting Materials and Methods for additional details.

Influenza virus preparation

Influenza A virus (strain X-31, A/Aichi/68, H3N2) was purchased from Charles River Laboratories (Wilmington, MA). For lipid mixing experiments, virus was labeled with the lipophilic dye TR-DHPE at a self-quenched concentration as described in the Supporting Methods. Varying the amount of TR-DHPE added to the virus threefold did not substantially alter the lipid mixing kinetics (see Fig. S5), indicating that this concentration of TR-DHPE minimally affected the lipid mixing process.

To incorporate DNA-lipids into viral particles for lipid-mixing experiments, DNA-lipids (sequence D) in deionized water were added to the suspension of dye-labeled virus particles at the following estimated DNA-lipid/viral particle ratios: 54 (1X), 108 (2X), 216 (4X). The virus suspension/DNA-lipid mixture was then incubated overnight at 4°C to allow DNA-lipid incorporation into the viral envelope. Because the viral particle concentration (and consequently DNA-lipid ratio) is only roughly estimated (see Supporting Materials and Methods), we use the labels of 1X, 2X, etc. for DNA-lipid concentration data. The observed distributions of DNA-lipids in viral particles at the various DNA-lipid concentrations, see Fig. 4.

Lipid mixing kinetic measurements

Following preparation of DNA-tethered vesicles and pH indicator membranes inside the flow cell, 5–20 μL of Texas Red-labeled virus particles (estimated viral particle concentration ~0.6 nM) were mixed into the flow cell, and incubated until a suitable density of bound virus particles was observed by fluorescence microscopy (typically ~15 min for GD1a-bound viruses, and ~60–120 min for DNA-bound viruses). The flow cell was then rinsed with at least 1 mL of Vesicle Buffer at 400 μL/min, the syringe pump was stopped, and any residual buffer in the buffer well was removed by pipette. To observe viral lipid mixing, a video micrograph in the Texas Red channel was initiated, 350 μL of Fusion Buffer (pH 5.0) was immediately added to the buffer well, and the syringe pump was started at 400 μL/min, pulling through 0.19 mL (the equivalent of ~9–10× flow cell volumes) over the course of ~30 s before automatically stopping. The time to transition from pH 7.4 to pH 5.0 at the sample surface was monitored by bleed-through fluorescence of the pH indicator membranes, and was typically ~1–2 s. Lipid mixing was observed for each viral particle via dequenching of TR-DHPE upon lipid transfer from viral envelope to target vesicle (e.g., example trace; see Fig. 5). The video micrograph was collected for 1000 video frames at 288 ms/frame.

Video micrographs were analyzed using custom-built scripts to identify lipid-mixing events and measure the waiting time between pH drop and the onset of lipid mixing for each event. Scripts are available at https://github.com/kassonlab/micrograph-spot-analysis; see Supporting Materials and Methods for additional image analysis details.

Virus binding experiments

Virus binding experiments (e.g., Fig. 3) were performed to glass-supported bilayers formed inside flow cells via the vesicle fusion technique using vesicles prepared without GD1a, but with the indicated sequence and concentration of DNA-lipid (see *Supporting Materials and Methods* and the schematic in Fig. S3). Glass-supported bilayers were used as the target membranes instead of DNA-tethered vesicles because of their lateral homogeneity. For each binding experiment, 15 μL of Texas Red-labeled virus suspension (estimated viral particle concentration ~0.6 nM) with the indicated concentration of DNA-lipid (sequence D) was mixed into each flow cell, and incubated for 50 min with occasional mixing. Flow cells were

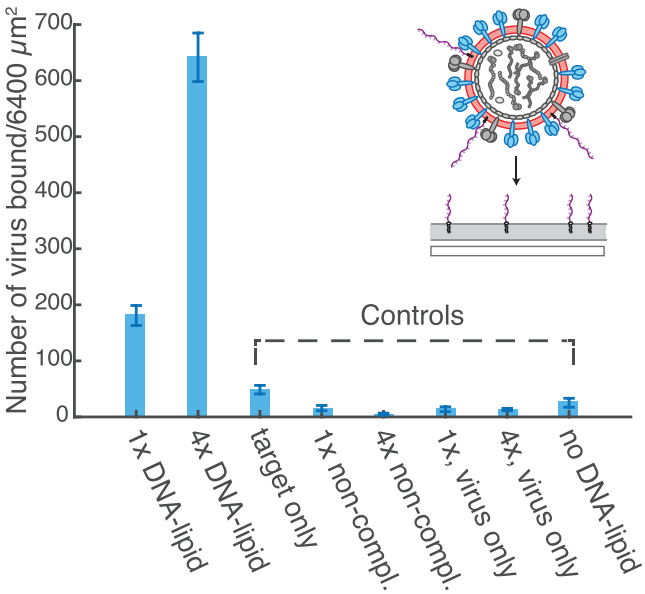

FIGURE 3 X-31 influenza virus particles are tethered specifically to target glass-supported lipid bilayers by DNA-lipids. Texas Red-labeled influenza virions (with or without DNA-lipids) were incubated above a glass-supported bilayer (SLB, displaying or not displaying the complementary DNA-lipids) inside a flow cell. Following removal of unbound virions by rinsing, the number of bound virus particles per microscope field of view (~6400 μm^2) was quantified by fluorescence microscopy. DNA-lipid sequences and concentrations were as follows. 1X DNA-lipid = 0.05 mol % sequence C (SLB), 1X sequence D (virus); 4X DNA-lipid = 0.05 mol % sequence C (SLB), 4X sequence D (virus); target only = 0.05 mol % sequence C (SLB), no DNA-lipid (virus); 1X non-compl. = 0.05 mol % sequence F (SLB), 1X sequence D (virus); 4X non-compl. = 0.05 mol % sequence F (SLB), 4X sequence D (virus); 1X, virus only = no DNA-lipid (SLB), 1X sequence D (virus); 4X, virus only = no DNA-lipid (SLB), 4X sequence D (virus); no DNA-lipid = no DNA-lipid (*both*). Schematic inset shows an influenza virion labeled with Texas Red (*red*) and displaying DNA-lipids (*purple*) binding to a glass-supported bilayer (*gray*) displaying the complementary DNA-lipids. To see this figure in color, go online.

then rinsed with 1.5 mL of Vesicle Buffer at 800 μL/min. Images of bound virus, and the underlying glass-supported bilayer, were then captured by fluorescence microscopy. The numbers of bound virus in each image were quantified via MATLAB scripts (The MathWorks, Natick, MA) available at https://github.com/kassonlab/micrograph-spot-analysis. See the Supporting Materials and methods for additional image analysis details.

Quantification of DNA-lipid distributions in viral particles

We characterized the DNA-lipid distributions in our virus particles (Fig. 4) by single-molecule photobleaching and two-color quantitative fluorescence imaging (see the schematic in Fig. S4). For these measurements, virus was prepared as previously mentioned, but with the following differences. Alexa 546-labeled DNA-lipids (sequence E) were incorporated into influenza virions instead of sequence D to enable quantitative fluorescence imaging. OG-DHPE was used to label the viral envelope instead of TR-DHPE because Alexa 546 has significant spectral overlap with Texas Red. Virus particles were labeled using an OG-DHPE/HB buffer solution at 3x lower concentration (i.e., a 1:120 ratio instead of 1:40).

Following preparation, viral particles with DNA-lipids were introduced into a flow cell on a clean glass coverslip and observed by fluorescence microscopy until a suitable density had bound nonspecifically to the glass surface. The flow cell was rinsed extensively with Vesicle Buffer. Images of viral particles (Oregon Green) and associated DNA-lipids (Alexa 546) were then recorded sequentially. To determine the intensity per Alexa 546 fluorophore, single step photobleaching video micrographs were also recorded using identical Alexa 546 imaging settings (Fig. S6). The observed bleedthrough of Oregon Green fluorescence into the Alexa 546 channel was negligible. Note that the integrity of the viral particle may be compromised upon adhering to the glass surface, however this should not influence the quantification, because the number of DNA-lipids in each viral particle should not be altered by this process.

We analyzed viral particle and Alexa 546-labeled DNA-lipid images, as well as single step photobleaching video micrographs via scripts available at https://github.com/kassonlab/micrograph-spot-analysis. We determined the Alexa 546 intensity per viral particle (directly proportional to the number of DNA-lipids) and calculated the Alexa 546 intensity per dye. The number of DNA-lipids in each viral particle was calculated by dividing the Alexa 546 intensity per viral particle by the average intensity per Alexa 546 dye. See Supporting Materials and Methods for additional analysis details.

RESULTS AND DISCUSSION

Virus tethering to target-supported lipid bilayers by DNA-lipid hybridization

Our strategy to bind virus particles to target membranes in the absence of receptor uses synthetic DNA-lipid conjugates, which spontaneously incorporate into lipid bilayers and have previously been shown to tether membranes to each other or to solid supports upon hybridization (13–16). To ascertain whether DNA-lipids could tether influenza virions to target membranes in the absence of receptors, we performed a quantitative binding assay to observe tethering between viruses with DNA-lipids and a target glass-supported bilayer displaying the complementary DNA strand (Fig. 3). X-31 influenza virions, fluorescently labeled with TR-DHPE and displaying DNA-lipids (sequence D), were introduced into a flow cell above a glass-supported bilayer displaying the complementary DNA strand, and incubated for 50 min. The flow cell was then rinsed extensively to remove any unbound or loosely bound virions, and the number of bound virions was then observed by fluorescence microscopy and quantified by image processing.

We observed that DNA-lipids could specifically tether virus particles to the supported bilayer. When complementary

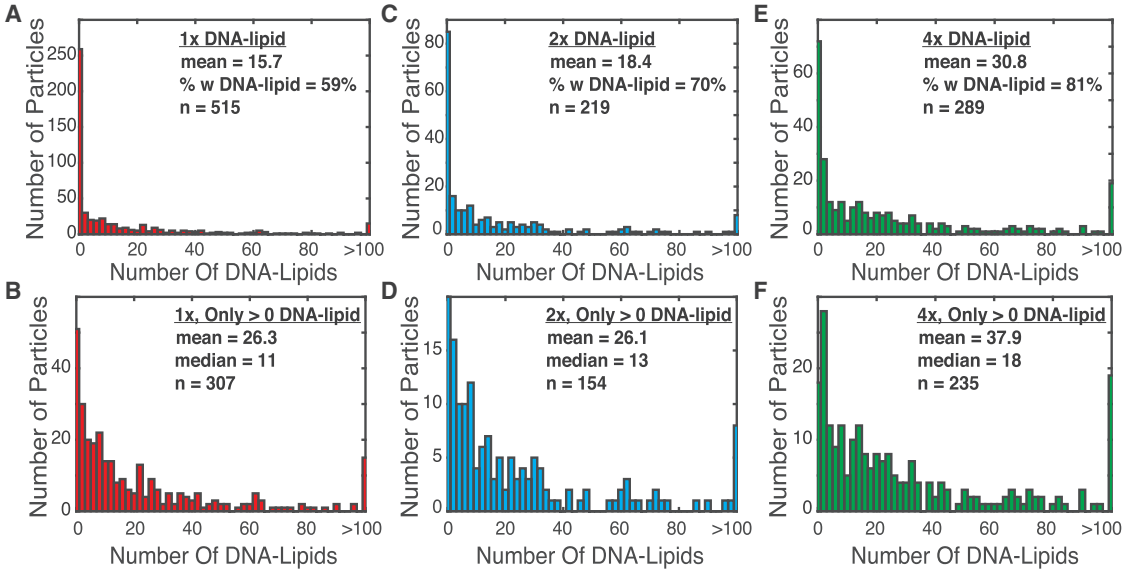

FIGURE 4 Observed DNA-lipid distributions in Oregon Green-labeled X-31 influenza virus particles incubated with 1× (*A* and *B*), 2× (*C* and *D*), or 4× (*E* and *F*) concentration of Alexa 546-labeled DNA-lipids (sequence E). (*A*), (*C*), and (*E*) show the observed DNA-lipid distributions in all virus particles (identified by Oregon Green fluorescence). (*B*), (*D*), and (*F*) show the DNA-lipid distributions only for those viral particles that contained at least 1 DNA-lipid. The number of DNA-lipids was determined from the Alexa 546 intensity colocalized with each virus particle, divided by the average intensity per Alexa 546 dye (see Fig. S6). To see this figure in color, go online.

DNA-lipids were incorporated into the virus particles and target bilayer, virions were stably bound to the bilayer following rinsing, and were not observed to disassociate from the target membrane, consistent with our previous reports of using DNA-lipids to bind large unilamellar vesicles to glass-supported bilayers (14,16). Virus tethering was also observed to be dependent on DNA-lipid concentration added to the virus—as more DNA-lipid was added to the virions, more virions were observed to bind to the target bilayer. Conversely, little tethering was observed in the absence of DNA-lipids on either membrane or with noncomplementary DNA-lipids. Additionally, no Texas Red signal was observed to be transferred from virus particles to the target glass-supported bilayers, indicating that DNA-lipid tethering of virus particles did not induce membrane fusion between virus and target bilayer.

Characterization of DNA-lipid incorporation into influenza virions

To characterize the DNA-lipid distributions in viral particles, we incorporated Alexa 546-labeled DNA-lipids into OG-DHPE-labeled virions and measured the number of DNA-lipids per virion by quantitative fluorescence imaging (Fig. 4). Virions were adhered nonspecifically to a clean glass coverslip, and then imaged to quantify the total Alexa 546 intensity associated with each viral particle, whose location was identified by Oregon Green fluorescence. This Alexa 546 intensity value is proportional to the number of DNA-lipids incorporated into each viral particle. To estimate the actual number of DNA-lipids in each viral particle, single-molecule photobleaching was used to determine the average fluorescence intensity per Alexa 546 dye (Fig. S6). The number of DNA-lipids in each viral particle was then calculated by dividing the total Alexa 546 intensity associated with each viral particle by the average intensity per Alexa 546.

As expected, we observed that the distribution of DNA-lipids incorporated into viral particles (Fig. 4) shifted to higher values as we increased the concentration of DNA-lipid added to the virions. We also observed that the proportion of virions displaying DNA-lipids increased with increasing DNA-lipid concentration. These two observations are consistent with the results from our binding assay (Fig. 3), in which we observed that increasing the DNA-lipid concentration added to the virus suspension from 1X to 4X and resulted in an increased number of viral particles bound to the target-supported bilayer, which displayed the complementary DNA-lipid.

We also observed that the distributions of DNA-lipids per viral particle had very long tails, suggesting that DNA-lipid incorporation into virus particles may largely be governed by the fusion of DNA-lipid micelles with the viral envelope rather than individual DNA-lipids that would be expected to give Poisson statistics; a similar result was previously observed for addition to pure lipid vesicles (20). Additionally, free DNA-lipids (Alexa 546 spots not colocalized with an Oregon Green spot) were observed at all concentrations of DNA-lipid added, even though there was a substantial population of virus particles with no DNA-lipids. This suggests that DNA-lipid incorporation into the virus particles is nonuniform. Efforts to facilitate more uniform incorporation of DNA-lipids into virus particles are ongoing, but nonuniform DNA-lipid incorporation did not detectably affect the influenza lipid mixing kinetics observed in our single virus lipid mixing assay, although we cannot rule out the possibility that it does affect lipid mixing efficiency (see below).

DNA-tethered vesicle target membranes and single virus lipid mixing assay

To examine the influence of native receptor binding on influenza virus fusion, we used a single virus lipid mixing assay where virions were bound to target DNA-tethered vesicles by either DNA-lipid tethering or native receptor binding. This single virus lipid mixing assay uses DNA-lipid conjugates in two separate ways: 1) to construct the surface-immobilized vesicles used as the targets for fusion and 2) to tether influenza virions to the target vesicles in the absence of any sialic acid containing receptors.

To construct the target vesicles, DNA-lipids are incorporated into large unilamellar vesicles (*green DNA strands* in Fig. 1) that are then tethered by hybridization to a substrate displaying the complementary DNA strand inside a flow cell. The length of the DNA duplex distances the vesicles (~8 nm for a 24-mer duplex) from the substrate, minimizing unwanted membrane-substrate interactions; the remainder of the surface is passivated to prevent membrane assembly. Similar membrane architectures have been employed in other fusion studies (21,22).

To study influenza (hemi-)fusion in the presence of receptor, the tethered vesicles are prepared with sialic acid-containing glycolipids (ganglioside GD1a, *black glycolipids* in Fig. 1). Virions labeled with TR-DHPE at a self-quenched concentration are introduced into the flow cell, and binding to tethered vesicles is observed by fluorescence microscopy. Unbound or loosely bound virions are then removed by extensive rinsing of the flow cell. Fusion is then initiated by buffer exchange to pH 5.0, approximating the pH drop inside the endosome, and lipid mixing for individual viruses is observed by fluorescence dequenching as lipids are transferred from viral envelope to target vesicle. The timing of the pH drop is monitored in situ via the fluorescence intensity of DNA-tethered pH indicator membranes present in each microscope field of view (see Materials and Methods section). An example video showing several lipid mixing events is shown in Movie S1, and an example lipid-mixing trace is shown in Fig. 5 *A*. The waiting time between pH drop and fluorescence dequenching captures the lipid

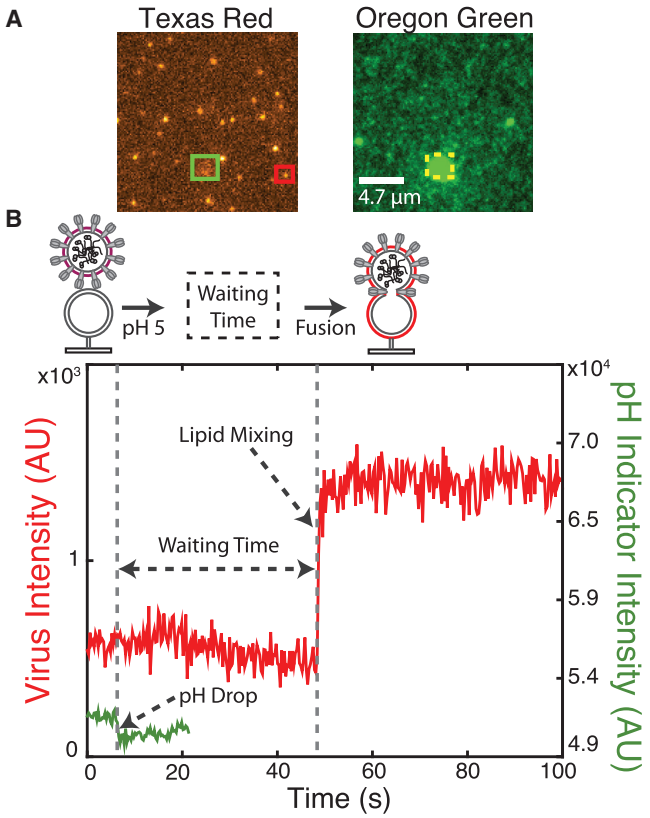

FIGURE 5 (*A*) Example images of Texas Red-labeled influenza virions bound to DNA-tethered vesicles by GD1a engagement before pH drop, and of an Oregon Green-labeled pH indicator membrane. The images are of the same field of view. The pH indicator membrane (*yellow box*) exhibits bleedthrough fluorescence (*green box*) in the Texas Red channel, which is used to monitor pH drop. The dim background in the Oregon Green channel is due to the DNA-tethered vesicles that are densely packed on the surface. Movie S1 shows the lipid mixing events that occur in this field of view. (*B*) Example fluorescence intensity time trace of a single virion (*red trace*, corresponding to the *red box* in *A*). Lipid mixing is identified as the rapid increase in fluorescence due to dequenching of the lipid dye in the viral envelope upon dilution into the target vesicle. The waiting time is the time between pH drop and lipid mixing. Bleedthrough fluorescence of the pH indicator membrane (*green trace*, corresponding to *green box* in *A*) is used to identify the pH drop. The schematic above the graph depicts the experiment—the virus (*dark red*) is bound to the target DNA-tethered vesicle (*gray circle*) before pH drop, and upon lipid mixing/fusion the lipid dye undergoes fluorescence dequenching (*bright red*). This schematic is only intended to illustrate the experiment and is not our proposed model for viral fusion. To see this figure in color, go online.

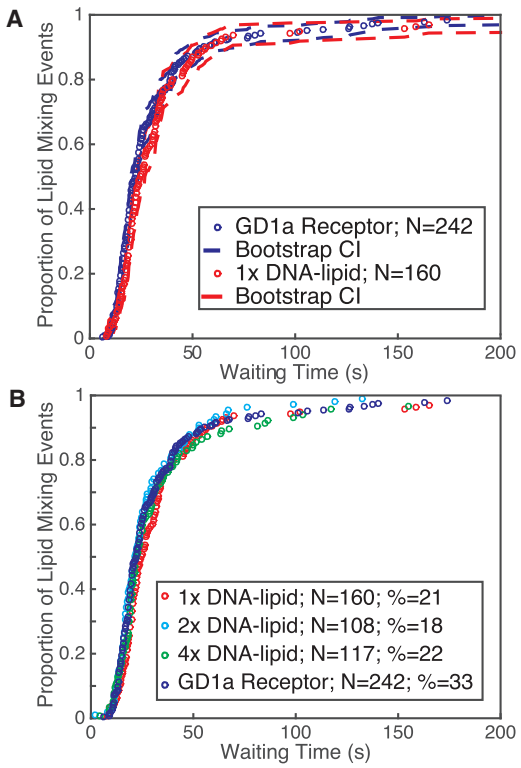

FIGURE 6 Lipid mixing kinetics of X-31 influenza virions bound to target vesicles by GD1a receptor binding or by DNA-lipid tethering are indistinguishable. (*A*) CDFs of lipid-mixing waiting time distributions for single-virus fusion events, together with bootstrap resampling error estimates (95% confidence intervals). (*B*) Lipid-mixing waiting time CDFs showing lack of concentration dependence of DNA-lipid added to influenza virions. The target vesicles in these experiments contain 0.03 mol % Sequence C (or an estimated ~30 DNA-lipids/vesicle for 100 nm vesicles). Virions contain Sequence D DNA-lipids at the concentration indicated. To see this figure in color, go online.

mixing kinetics. To quantify the kinetics for this lipid mixing process, individual waiting times from the entire cohort of events are compiled into a cumulative distribution function (CDF) (e.g., Fig. 6).

To study influenza lipid mixing in the absence of receptor, DNA-lipids are incorporated into the viral envelope and target vesicles (*purple DNA strands* in Fig. 1). Hybridization between complementary strands binds the virus to the target vesicle in the absence of receptor. Following virus tethering to the target vesicle, fusion is then triggered and studied as previously mentioned.

We note that an important feature of our single virus lipid mixing assay (as with other single virus fusion assays) is that only prebound virions are monitored for fusion events because all unbound virions are removed by rinsing the flow cell before triggering fusion by pH drop. This removes any contribution to the (hemi-)fusion kinetics from unbound virions where the waiting time would be convolved with diffusion, potentially confounding the results. We also note that while in the assay described herein we only examine lipid mixing (which would occur for both hemifusion and full fusion), a bulk fusion assay performed in solution by our laboratory shows both lipid and contents mixing between X-31 influenza virions and similar large unilamellar vesicles, suggesting that full fusion also likely occurs here (23).

Influenza virus lipid mixing kinetics do not depend on native receptor binding

We used our DNA-lipid tethering strategy, in conjunction with the single virus lipid mixing assay, to examine the

influence of receptor binding on influenza virus (hemi-) fusion. To do this, we performed single virus lipid mixing measurements on virions bound to target tethered vesicles either by HA-GD1a binding or by DNA-lipid tethering, as shown schematically in Fig. 1. We then compared the lipid mixing waiting time distributions for virions bound by GD1a binding or by DNA-lipid tethering (Fig. 6 *A*). Interestingly, we observed that viral lipid mixing kinetics were the same within experimental error regardless of whether the virus was bound to the target by GD1a engagement or by DNA-lipid tethering. This observation supports the hypothesis that receptor binding does not influence the mechanism of influenza virus lipid mixing in a way that alters the rate-limiting step, because the lipid mixing kinetics of virions bound to target membranes in the absence of receptor (i.e., with DNA-lipids) were identical to the kinetics of virions bound to receptor (i.e., to GD1a). More specifically, this indicates that if receptor binding induces hemagglutinin clustering and/or other spatial rearrangements on the virion, these rearrangements do not alter the subsequent pH-triggered lipid mixing kinetics. We highlight that this inference strictly only applies to the rate-limiting step(s) of lipid mixing, which is the observable in our single virus measurements. We cannot make any direct claims about the influence of receptor binding on any fast steps that may precede lipid transfer, or any subsequent steps involved in content transfer, which we are not observing.

A prediction from this inference would be that the lipid mixing kinetics should not depend on the GD1a concentration in the target membrane. To test this, we compared the waiting time distributions from single virus lipid mixing events, where the virions were bound to the target DNA-tethered vesicles containing either 1% or 2% GD1a (Fig. S7). We observed that the lipid mixing kinetics were identical, consistent with the hypothesis that receptor binding does not influence lipid mixing kinetics. We also note that the kinetics observed in our assay are similar to previous measurements of single X-31 influenza lipid mixing events at similar pH values, but with different target membrane architectures and lipid compositions (7,12).

We next examined the influence of DNA-lipid concentration added to the viral envelope on the lipid mixing kinetics. We observed that the kinetics remained unchanged as the amount of DNA-lipid added to the viral envelope increased fourfold (Fig. 6 *B*). This suggests that the lipid mixing kinetics are not greatly influenced either by the DNA-lipid concentration in the viral envelope, or by the nonuniform distribution of DNA-lipids per virion. Both of these observables change with DNA-lipid concentration added to the virus (Fig. 4), and yet the lipid mixing kinetics remain unchanged.

On the other hand, the efficiency of lipid mixing was somewhat lower for virus particles tethered by DNA-lipids (~20%) as compared to those bound to GD1a (~30%). This could indicate that the DNA-lipid hybrids responsible for tethering may inhibit fusion for some viral particles. Indeed, it seems reasonable to assume that virions that contain a high number of DNA-lipids (i.e., those in the long tail of the DNA-lipid per virion distributions shown in Fig. 4) might be sterically hindered from undergoing a fusion transition. Alternatively, perhaps the DNA-lipids that are unincorporated into the virions could prevent fusion through some mechanism. However, neither of these explanations appears to be fully consistent with the observation that the efficiency of lipid mixing remained constant from 1X to 4X DNA-lipid added to the viral envelope, even though the proportion of virions in the tail of the distribution increases with increasing DNA-lipid concentration, as shown in Fig. 4, and the concentration of unincorporated DNA-lipids also increases.

An alternative explanation for the decreased lipid mixing efficiency is that DNA-lipid tethering may successfully capture fusion-defective virus particles, which cannot undergo binding to GD1a and would thus be unobserved in the GD1a lipid mixing measurements, thus increasing the apparent lipid mixing efficiency for virions bound to target vesicles by GD1a. It would be challenging to disentangle these explanations and they are not mutually exclusive. For this reason, and because the change in efficiency is not large, we focus our conclusions on the lipid mixing kinetics rather than on efficiency.

CONCLUSIONS

We have presented a strategy to use synthetic DNA-lipids to tether X-31 influenza virions to artificial target membranes in the absence of viral receptor. This general method enables biophysical studies of the role of receptor binding in viral membrane fusion. We expect that it should be broadly applicable to other enveloped viruses, and be particularly useful to study viruses where the receptor is unknown or challenging to reconstitute. Additionally, this strategy enables deconvolution of differences in fusion from receptor binding avidity between viral strains, allowing for more direct comparisons between strains. DNA-lipid tethering should thus enable mechanistic study of membrane fusion in a broader range of viruses than via previous methods. Applying this technique to X-31 influenza virus, we have demonstrated that the single virus lipid mixing kinetics appear to be independent of receptor binding, because the kinetic distributions measured from virions bound by GD1a or by DNA-lipid were identical within experimental error. This suggests that receptor binding does not cause any inter- or intrasubunit reorganization of HA affecting the rate-limiting steps of pH-triggered lipid mixing. This provides evidence for a common yet previously unproven assumption regarding influenza fusion and shows how such a technique can be used to investigate other viruses where receptor binding may indeed cluster viral fusion proteins to facilitate fusion.

SUPPORTING MATERIAL

Supporting Materials and Methods, seven figures, one table, and one movie are available at http://www.biophysj.org/biophysj/supplemental/S0006-3495(16)30395-2.

AUTHOR CONTRIBUTIONS

R.J.R., P.M.K., and S.G.B. designed the research. R.J.R. performed the research and analyzed the data. R.J.R., P.M.K., and S.G.B. wrote the article. P.M.K. and S.G.B. contributed material resources.

ACKNOWLEDGMENTS

We thank Isabel Goronzy (Stanford) for performing the viral protein concentration measurements and for helpful discussions. We thank Dr. Peter Kim (Stanford) for useful discussions and Elizabeth Webster (Stanford) for manuscript feedback.

This work was funded by National Institutes of Health (NIH) grant R01 GM098304 to P.M.K., a collaborative supplement to that award, and NIH grant R01 GM069630 to S.G.B.

SUPPORTING CITATIONS

References (24–26) appear in the Supporting Material.

REFERENCES

1. Harrison, S. C. 2008. Viral membrane fusion. *Nat. Struct. Mol. Biol.* 15:690–698.
2. Eckert, D. M., and P. S. Kim. 2001. Mechanisms of viral membrane fusion and its inhibition. *Annu. Rev. Biochem.* 70:777–810.
3. Blumenthal, R., S. Durell, and M. Viard. 2012. HIV entry and envelope glycoprotein-mediated fusion. *J. Biol. Chem.* 287:40841–40849.
4. Skehel, J. J., and D. C. Wiley. 2000. Receptor binding and membrane fusion in virus entry: the influenza hemagglutinin. *Annu. Rev. Biochem.* 69:531–569.
5. White, J. M., and K. L. Schornberg. 2012. A new player in the puzzle of filovirus entry. *Nat. Rev. Microbiol.* 10:317–322.
6. Brecher, M., K. L. Schornberg, …, J. M. White. 2012. Cathepsin cleavage potentiates the Ebola virus glycoprotein to undergo a subsequent fusion-relevant conformational change. *J. Virol.* 86:364–372.
7. Floyd, D. L., J. R. Ragains, …, A. M. van Oijen. 2008. Single-particle kinetics of influenza virus membrane fusion. *Proc. Natl. Acad. Sci. USA.* 105:15382–15387.
8. Ivanovic, T., J. L. Choi, …, S. C. Harrison. 2013. Influenza-virus membrane fusion by cooperative fold-back of stochastically induced hemagglutinin intermediates. *eLife.* 2:e00333.
9. Chao, L. H., D. E. Klein, …, S. C. Harrison. 2014. Sequential conformational rearrangements in flavivirus membrane fusion. *eLife.* 3:e04389.
10. Niles, W. D., and F. S. Cohen. 1991. Fusion of influenza virions with a planar lipid membrane detected by video fluorescence microscopy. *J. Gen. Physiol.* 97:1101–1119.
11. Wessels, L., M. W. Elting, …, K. Weninger. 2007. Rapid membrane fusion of individual virus particles with supported lipid bilayers. *Biophys. J.* 93:526–538.
12. Costello, D. A., D. W. Lee, …, S. Daniel. 2012. Influenza virus-membrane fusion triggered by proton uncaging for single particle studies of fusion kinetics. *Anal. Chem.* 84:8480–8489.
13. Chan, Y.-H. M., B. van Lengerich, and S. G. Boxer. 2008. Lipid-anchored DNA mediates vesicle fusion as observed by lipid and content mixing. *Biointerphases.* 3:FA17–FA21.
14. van Lengerich, B., R. J. Rawle, and S. G. Boxer. 2010. Covalent attachment of lipid vesicles to a fluid-supported bilayer allows observation of DNA-mediated vesicle interactions. *Langmuir.* 26:8666–8672.
15. Chung, M., R. D. Lowe, …, S. G. Boxer. 2009. DNA-tethered membranes formed by giant vesicle rupture. *J. Struct. Biol.* 168:190–199.
16. Yoshina-Ishii, C., and S. G. Boxer. 2003. Arrays of mobile tethered vesicles on supported lipid bilayers. *J. Am. Chem. Soc.* 125:3696–3697.
17. Hutchinson, E. C., P. D. Charles, …, E. Fodor. 2014. Conserved and host-specific features of influenza virion architecture. *Nat. Commun.* 5:4816.
18. Ivanovic, T., and S. C. Harrison. 2015. Distinct functional determinants of influenza hemagglutinin-mediated membrane fusion. *eLife.* 4:e11009.
19. Hughes, L. D. 2013. Model membrane architectures for the study of membrane proteins. Doctoral Dissertation. Stanford University. https://purl.stanford.edu/xr495nv6897. Accessed December 17, 2015.
20. van Lengerich, B., R. J. Rawle, …, S. G. Boxer. 2013. Individual vesicle fusion events mediated by lipid-anchored DNA. *Biophys. J.* 105:409–419.
21. Kyoung, M., A. Srivastava, …, A. T. Brunger. 2011. In vitro system capable of differentiating fast Ca2+-triggered content mixing from lipid exchange for mechanistic studies of neurotransmitter release. *Proc. Natl. Acad. Sci. USA.* 108:E304–E313.
22. Diao, J., Y. Ishitsuka, …, T. Ha. 2012. A single vesicle-vesicle fusion assay for in vitro studies of SNAREs and accessory proteins. *Nat. Protoc.* 7:921–934.
23. Domanska, M. K., D. Wrona, and P. M. Kasson. 2013. Multiphasic effects of cholesterol on influenza fusion kinetics reflect multiple mechanistic roles. *Biophys. J.* 105:1383–1387.
24. Domanska, M. K., R. A. Dunning, …, P. M. Kasson. 2015. Hemagglutinin spatial distribution shifts in response to cholesterol in the influenza viral envelope. *Biophys. J.* 109:1917–1924.
25. Shrirao, A. B., A. Hussain, …, R. Perez-Castillejos. 2012. Adhesive-tape soft lithography for patterning mammalian cells: application to wound-healing assays. *Biotechniques.* 53:315–318.
26. Pähler, G., C. Panse, …, A. Janshoff. 2012. Coiled-coil formation on lipid bilayers—implications for docking and fusion efficiency. *Biophys. J.* 103:2295–2303.

Biophysical Journal, Volume *111*

Supplemental Information

Disentangling Viral Membrane Fusion from Receptor Binding Using Synthetic DNA-Lipid Conjugates

Robert J. Rawle, Steven G. Boxer, and Peter M. Kasson

Table of Contents

Labeled Schematic of Influenza Virus

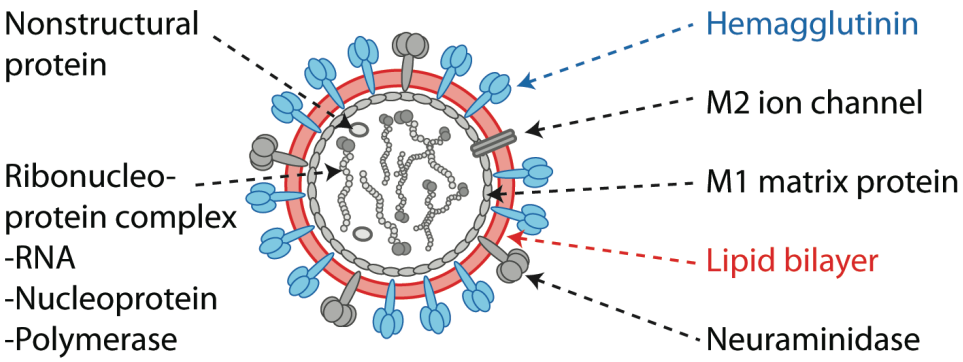

Figure S1. *Schematic of influenza virus components. The lipid envelope is drawn in red to indicate the presence of a lipid dye (e.g. Texas Red-DHPE) which has been externally incorporated into the membrane. Presumably the lipid dye is located largely if not exclusively in the outer membrane leaflet. Hemagglutinin (light blue) is the viral membrane protein responsible both for receptor binding and for mediating membrane fusion.*

Supporting Methods

Additional Microscopy Details

Texas Red and Alexa 546 images used a Texas Red filter cube (ex = 562/40 nm, bs = 593 nm, em = 624/40 nm), and additional excitation (ex = 560/55 nm) and emission (em = 645/75 nm) filters. Oregon Green images used a NBD filter cube (ex = 475/35 nm, bs = 509 nm, em = 528/38 nm), and additional excitation (ex = 460/50 nm) and emission (em = 535/50 nm) filters. Lipid mixing video micrographs were captured at 288 ms/frame. Alexa 546 images and single-step photobleaching videos were captured at 500 ms/frame.

Alkyne-DNA Functionalization and Dye-DNA-lipid Conjugation

Alkyne-terminated DNA (Sequence B) was prepared by the Protein and Nucleic Acid Facility at Stanford University, using the 5'-Hexynyl Phosphoramidite reagent from Glen Research (Sterling, VA), and was purified by HPLC upon receipt. This alkyne-DNA was used to prepare DNA-modified coverslips via alkyne-azide click chemistry.

Alexa 546-labeled DNA-lipid (Sequence E) was prepared by NHS coupling of Alexa 546-succinimidyl ester with a primary amine-terminated DNA-lipid as previously described [1], and purified by size exclusion. The calculated labeling efficiency, determined by absorbance at 554 nm and 260 nm (corrected according to manufacturer's instructions), was ~95%. This Alexa 546-DNA-lipid was used to determine the DNA-lipid distribution in viral particles (i.e. Figure 4 in Main Text).

Table S1. DNA-lipid and Alkyne-DNA Sequences Used

Name	DNA Sequence (5' to 3')	Complementary Sequence
A	lipid – TGC GGA TAA CAA TTT CAC ACA GGA	B
B	alkyne – TCC TGT GTG AAA TTG TTA TCC GCA	A
C	lipid – TAG TAT TCA ACA TTT CCG TGT CGA	D
D	lipid – TTT TTT TTT TTT TTT TTT TTT TTT TCG ACA CGG AAA TGT TGA ATA CTA	C
E	lipid – TTT TTT TTT TTT TTT TTT TTT TTT – Alexa 546	none
F	lipid – TTT TTT TTT TTT TTT TTT TTT TTT	none

Note that the DNA-lipid sequence incorporated into the virus in tethering and lipid mixing experiments (Sequence D) includes a 24mer poly T non-complementary linker on the membrane proximal side (see Table S1). This is intended to extend the complementary region away from the viral envelope, which is densely packed with membrane proteins [2,3], and to provide flexibility following binding, although we have not tested this directly.

Polydimethylsiloxane (PDMS) Flow Cell Design and Preparation

PDMS flow cells on microscope coverslips were used in all microscopy measurements and experiments herein (virus binding to glass supported bilayer, single virus lipid mixing assays, characterization of DNA-lipid distributions in virus, etc.). For reference, Figure S2 shows a schematic of our flow cell design, as well as a picture of an example flow cell. Each coverslip contained two independent flow cells, as shown.

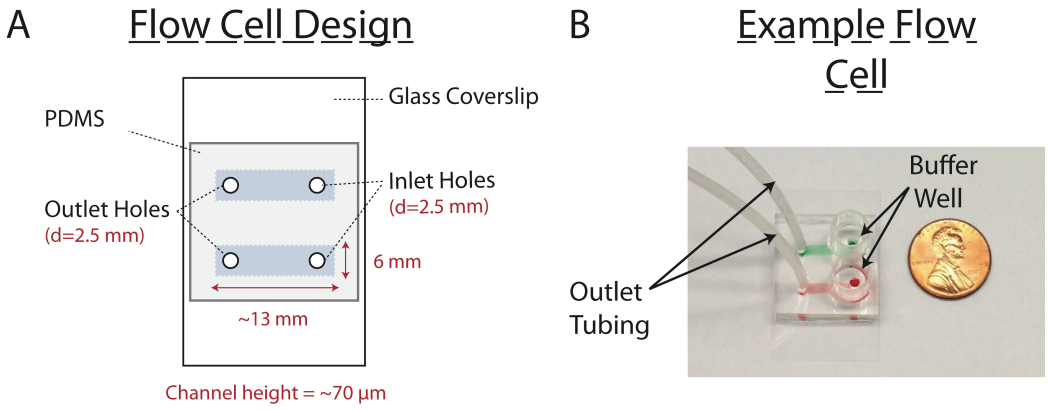

Figure S2*. (A) Schematic design of two channel PDMS flow cell on glass coverslip. (B) Photograph of example flow cell, filled with solutions of red and green food coloring for visualization.*

The "tape-based soft lithography" method was used for the preparation of the PDMS flow cells [4]. Specifically, simple flow cell molds were prepared by affixing small strips (6 mm x ~13 mm) of Kapton polyimide tape (Ted Pella Inc., Redding, CA) to a clean silicon wafer. To prevent PDMS adherence to the mold, the mold was silanized by vapor deposition of 200 μL of tridecafluoro-1,1,2,2-tetrahydrooctyltrichlorosilane in an adjacent dish under vacuum for 2 hours. PDMS was prepared by mixing together a 10:1 ratio of Sylgard 184 elastomer base: monomer (Ellsworth Adhesives, Germantown, WI) and degassing under house vacuum for 1h. The PDMS mixture was then poured on top of the mold and cured at 70°C for 2h. Pairs of flow cells were cut out with a scalpel, and inlet/outlet holes were punched with a biopsy hole puncher (2.5 mm diameter, Harris Uni-core, Ted Pella Inc.). Flow cell volume was ~20 μL. Sets of two flow cells were bonded directly to clean glass coverslips following a 60s exposure to air plasma (Harrick Plasma Cleaner PDC-3xG, Harrick Plasma, Ithaca, NY), or were affixed to azide-functionalized coverslips (discussed below) with five minute epoxy (Devcon, ITW Polymer Adhesives North America, Danvers, MA). For rapid exchange of solution inside the flow cell, a buffer well was created by gluing the cut end of a 1 mL plastic pipette tip over the inlet hole with five minute epoxy. Flow inside the cell was controlled by a syringe pump (KD Scientific, Holliston, MA) operating in suction mode, attached to the outlet hole by Intramedic polyethylene tubing (I.D. 1.67 mm, O.D. 2.42 mm). Where relevant, flow rates are listed.

Cleaning of glass coverslips

Glass coverslips (24 x 40 mm, No 1.5, VWR International, Randor, PA) were cleaned by immersing in a 1:7 solution of 7x detergent (MP Biomedicals, Burlingame, CA) and de-ionized water, and heating until clear. Coverslips were then rinsed extensively with de-ionized water, and then baked in a kiln at 400°C for 4 hours.

DNA-modified coverslip preparation

DNA-modified coverslips were used as the substrate to form the DNA-tethered vesicle assemblies used as targets in our single virus lipid mixing assay (see schematic in Figure 2 in the Main Text). These DNA-modified coverslips were prepared as previously described [1,5]. This process consists of first functionalizing a clean glass coverslip with an alkyl azide by silanization chemistry, then covalently coupling short DNA oligomers to the surface by the alkyne-azide click reaction. Subsequently, any unreacted azide groups remaining on the surface are passivated with ethynyl phosphonic acid (EP), also via the alkyne-azide click reaction.

Briefly, clean glass coverslips were silanized using 11-Azidoundecyltrimethoxysilane in a vapor deposition chamber, resulting in azide-functionalized coverslips. PDMS flow cells were affixed to the top of the functionalized coverslips with five-minute epoxy. To covalently attach DNA to the functionalized substrate surface, 24 μL of DNA-click cocktail was added to the flow cell and incubated for 90 minutes. DNA-click cocktail was prepared immediately beforehand and consisted of 60 μM alkyne-terminated DNA (Sequence B), 20 mM sodium ascorbate, 0.43 mM copper (II) sulfate, and 0.86 mM TTMA ligand. The flow cell was then rinsed with 1 mL de-ionized water, and any unreacted azide was then passivated with ethynyl phosphonic acid (EP) by mixing in 24 μL of EP-click cocktail and incubating for 90

minutes. EP-click cocktail was prepared immediately beforehand and consisted of 17 mM ethynyl phosphonic acid, 20 mM sodium ascorbate, 0.43 mM copper (II) sulfate, and 0.86 mM TTMA ligand. The flow cell was then rinsed with at least 1 mL de-ionized water. These DNA-modified coverslips could be stored overnight at 4°C. Immediately before using a flow cell, it was rinsed with several mL of Vesicle Buffer.

Vesicle preparation

A lipid mixture of 67.5% POPC, 20% DOPE, 10% cholesterol, 2% GD1a, and 0.5% Oregon Green-DHPE was prepared in chloroform in a glass test tube (140 nmol total lipids). For vesicles prepared without the influenza virus receptor, 2% GD1a was omitted and replaced with an additional 2% of POPC. Chloroform was evaporated under a stream of nitrogen gas, and then under house vacuum for at least 3h. The lipid film was then resuspended in Vesicle Buffer, and passed at least 20x through an extrusion membrane (100 nm pore size) using a mini-extruder (Avanti Polar Lipids) to yield large unilamellar vesicles. To prepare vesicles containing DNA-lipids, DNA-lipids in deionized water of the appropriate sequence were then added to the suspension of vesicles, and incorporated via an overnight incubation at 4°C. These vesicles could be stored at 4°C for several days.

pH Indicator Membrane Preparation

pH indicator membranes were used to accurately determine the timing of the pH drop at the sample surface in our lipid mixing experiments. These pH indicator membranes were DNA-tethered membrane patches, whose preparation we have described previously [1,5]. Essentially, their preparation entails rupturing giant unilamellar vesicles (GUV) which display DNA-lipid tethers onto DNA-modified coverslips which display the complementary DNA strand. The pH indicator membranes contain a high concentration of Oregon Green dye, which is pH sensitive across the pH range of our experiments.

To prepare the pH indicator GUVs, a lipid mixture of 64.5% POPC, 20% DOPE, 10% cholesterol, 5% Oregon Green-DHPE, and 0.5% DNA-lipid (Sequence A) was prepared in 1:1 chloroform: methanol in a glass scintillation vial, dried under a stream of nitrogen gas, and then under house vacuum for at least 3 h. GUVs were formed by adding 1.5 mL of 500 mM sucrose drop-wise, and then incubating overnight at 37°C. To prepare the pH indicator membranes inside our PDMS flow cells, 1 μL of a 1:10 dilution of the GUV solution in Vesicle Buffer was mixed into the flow cell during DNA-tethered target vesicle formation (see Methods in Main Text). Because of the high concentration (0.5%) of DNA-lipids in the GUVs, GUVs will tether by hybridization to the DNA-modified coverslip and eventually rupture to form planar tethered membranes patches that can then serve as pH indicators. This procedure resulted in a sufficiently low density of pH indicator membrane patches such that only a few pH indicator membranes were within a typical microscope field of view. Note that the bleed-through of the Oregon Green fluorescence from these pH indicator membranes into the Texas Red channel is sufficient to accurately observe the timing of the pH drop as a decrease in fluorescence without requiring a two-color fluorescence measurement (see example images and green trace in Figure 5 in the Main Text). In some lipid mixing data sets, pH indicator membranes were omitted, and the pH drop was estimated based on the time that flow was initiated to introduce the low pH Fusion Buffer into the flow cell. Based on

calibration experiments, the error introduced in these cases is approximately 1-2s (data not shown) and should not significantly impact our results.

Fluorescent Labeling of Influenza Virus

Texas Red-DHPE at 0.75 mg/mL in ethanol was mixed with HB buffer at a 1:40 ratio. 18 μL of influenza virus at 2 mg/mL (viral protein concentration provided by manufacturer) was mixed with 72 μL of Texas Red-DHPE/HB buffer solution, and incubated at RT for 2h while rocking. Labeled influenza virus was then isolated from any unincorporated Texas Red-DHPE by adding 1.3 mL of HB buffer, and pelleting the virus by centrifugation at 21,000 x g for 50 minutes. The pellet was resuspended in 20 μL of HB buffer, and left on ice at 4°C for at least several hours. The concentration of viral particles in this solution was estimated at ~2.8 nM, calculated from the viral protein concentration (see below). The labeled virus solution was then diluted 5x in HB buffer for use in lipid mixing experiments. This labeling procedure yields virus particles with a self-quenched concentration of Texas Red.

Estimation of Influenza Virus Concentration

The concentration of viral particles following Texas Red-DHPE labeling (see above) was roughly estimated by measuring the viral protein concentration using a BCA assay kit (ThermoFisher Scientific), and using an average protein MW per virus particle (1.8×10^8 Da) estimated from literature values of average copy numbers of viral proteins per virus particle [3]. For a typical preparation, viral protein concentration was measured at ~0.5 mg/mL, yielding an estimated viral particle concentration of ~2.8 nM.

Preparation of glass-supported bilayers for virus binding experiments

~20 μL of vesicle suspension in Vesicle Buffer (0.56 mM nominal total lipid concentration) was pipetted into a flow cell on a clean glass coverslip, and incubated for 30 min at RT to allow bilayer formation. Flow cells were then rinsed at 1000 μL/min with 1mL de-ionized water to dislodge nonspecifically bound vesicles, and then exchanged with at least 2 mL of Vesicle Buffer.

Image Analysis

Three different sets of custom-built Matlab scripts (MathWorks, Inc.) were used to analyze microscopy images and videos from our experiments: 1) Quantification of the number of virions bound to glass supported bilayers, 2) Analysis of single virus lipid mixing events, and 3) Characterization of the DNA-lipid distributions in viral particles. A brief overview of each set of image analysis scripts is described briefly below and all scripts are available at https://github.com/kassonlab/micrograph-spot-analysis upon publication.

1) Analysis of Virus Binding to Glass Supported Bilayers

Viral particles (labeled with Texas Red) which were bound to glass supported bilayers (labeled with Oregon Green) were identified by global thresholding of each Texas Red image. In essence, any pixels in the image above a certain threshold value (determined in relation to the background counts within each image) were identified as possible viral particles. The size, shape, and intensity of each of these possible viral

particles was then quantified. Very large/irregularly shaped particles (presumably many viral particles which have clumped together or other membrane debris left over from the viral prep by the manufacturer) were excluded. Regions near bright spots identified in the Oregon Green (glass supported bilayer) image were also excluded. These bright spots were presumably non-specifically bound vesicles left over from the supported bilayer formation process, and the inclusion or exclusion of these regions would not dramatically alter our data. The number of remaining viral particles per unit area was then calculated for each image. The data shown in Figure 3 is scaled to the size of approximately one field of view (~6400 μm^2).

2) Analysis of Single Virus Lipid Mixing Events

The general algorithm to analyze the video micrographs containing the single virus lipid mixing events from our assay was as follows. First, bound viral particles were found by global thresholding as above, excluding very large/irregularly shaped particles, as well as those near the edge of the field of view or too close to other viral particles. For each of the remaining viral particles, the background subtracted, integrated fluorescence intensity within a region of interest was then extracted for each video frame. These integrated intensity values were then compiled into a fluorescence time trace, such as the example trace shown in Figure 5 in the Main Text. Each fluorescence time trace was then analyzed to identify any lipid mixing events. Lipid mixing events were identified as a rapid increase in the fluorescence time trace, identified by a spike in the first derivative of the trace, as well as the magnitude of the fluorescence intensity change. Each viral particle was classified as having a) a lipid mixing event, b) no lipid mixing event, or c) an irregular lipid mixing event (e.g. multiple rapid fluorescence increases, slow fluorescence increase, etc.). The waiting time between pH drop and the onset of lipid mixing was then calculated for each lipid mixing event. pH drop was determined from the rapid drop in bleedthrough fluorescence of the pH indicator membrane (e.g. the green trace in Figure 5). Cumulative distribution functions (CDF) were compiled from the waiting times of individual lipid mixing events; irregular lipid mixing events were not included. Lipid mixing efficiency was calculated as the number of observed lipid mixing events divided by total number of virus particles analyzed.

3) Quantification of DNA-lipid Distributions in Viral Particles

Two sets of micrograph data were analyzed to characterize the DNA-lipid distributions in viral particles. First, single step photobleaching video micrographs of Alexa 546-labeled DNA-lipids incorporated into viral particles were analyzed to calculate the average Alexa 546 intensity per dye. Second, images of viral particles (Oregon Green images) and associated dye-labeled DNA-lipids (Alexa 546 images) were analyzed to determine the total Alexa 546 intensity associated with each virion. The number of DNA-lipids in each virion was calculated by dividing the total Alexa 546 intensity per viral particle by the average intensity per Alexa 546 dye.

To analyze the single step photobleaching video micrographs, Alexa 546 spots were manually chosen in each micrograph, specifically choosing only the dimmer spots (containing three or fewer dye molecules) to avoid complications from multiple overlapping photobleaching steps. The integrated fluorescence intensity time trace of these spots was recorded, and analyzed by a Bayesian change point inference script to

determine the number of photobleaching steps and step heights (see example trace and histogram of step heights in Figure S6). The correct identification of steps and step heights was verified by eye for each trace. Each step height value corresponds to the intensity per dye molecule, and the average Alexa 546 intensity per dye was calculated from all steps analyzed.

To determine the DNA-lipid distribution in viral particles, viral particle and DNA-lipid images were then analyzed. First, viral particles were identified by global thresholding in the Oregon Green image as above, excluding very large/irregularly shaped viral particles, those near the edge of the field of view or too close to other viral particles. Second, the integrated Alexa 546 intensity in the region of interest around each viral particle was recorded, after subtracting a local background value determined by fitting a 2D Gaussian to the Alexa 546 spot. Finally, the number of DNA-lipids in each viral particle was calculated by dividing the integrated Alexa 546 intensity by the average intensity per Alexa 546 dye, as determined by single step photobleaching.

Methods Schematics

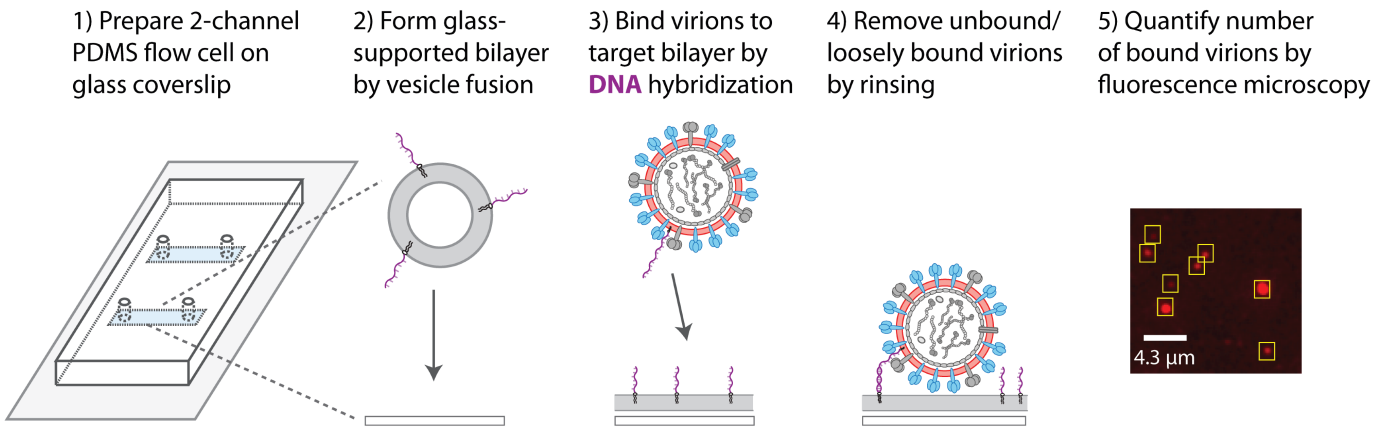

Figure S3. *Schematic of virus binding experiment, used to demonstrate that DNA-lipids can specifically tether influenza virions to target membranes. The image shown in step 5 is an example image (Texas Red channel) of influenza virions bound to a glass supported bilayer. See details in the Methods section of the main text and data in Figure 3.*

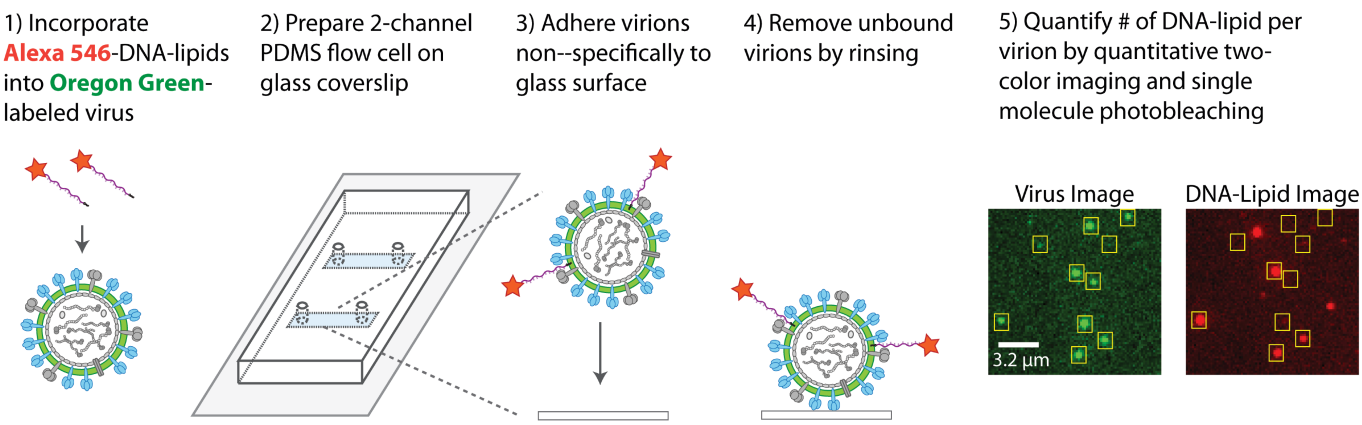

Figure S4. *Schematic of measurement to quantify the number of DNA-lipids incorporated into influenza virions. Images shown in step 5 are example images in the Oregon Green (virus) and Alexa 546 (DNA-lipid) channels. See details in the Methods section of the main text, and data in Figures 4 & S6.*

Supporting Data

Influence of Texas Red-DHPE Concentration on Viral Lipid Mixing Kinetics

Texas Red-DHPE was used to label the influenza virus envelope at self-quenched concentrations for all lipid mixing experiments performed in this report. Texas Red-DHPE is known to exhibit self-quenching at concentrations of ~3-5% in model lipid membranes [6]. However, because we only have an estimate of the viral particle concentration (see above) and since we do not know the incorporation rate of Texas Red-DHPE into our viral membranes, we do not have a direct measure of the Texas Red-DHPE concentration in our labeled virus particles. We only observe empirically that a self-quenched concentration of Texas Red-DHPE has been reached. To rule out the possibility that the concentration of Texas Red-DHPE used in our experiments might substantially perturb the lipid mixing measurements, we varied the concentration of Texas Red added during the virus labeling procedure threefold. Specifically, the ratio of Texas Red-DHPE : HB buffer used in the labeling procedure (see Methods in Main Text) was varied from 1:120 to 1:80 to 1:40 (i.e. 1X to 3X in the legend in Figure S5). We then measured the lipid mixing kinetics for each concentration of Texas Red-DHPE using our single virus lipid mixing assay. We observed that the lipid mixing kinetics for each Texas Red concentration were identical within error (see Figure S5), suggesting that Texas Red-DHPE was minimally perturbative to the lipid mixing process across this concentration range.

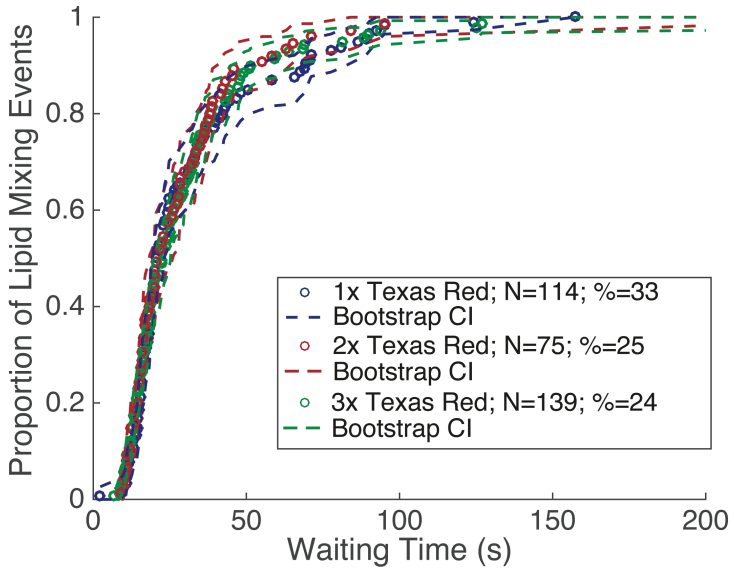

Figure S5. *Varying the Texas Red-DHPE added to the viral envelope threefold does not substantially alter the lipid mixing kinetics. CDFs of lipid-mixing waiting time distributions for single-virus fusion events are shown, together with bootstrap re-sampling error estimates (95% Confidence Intervals).*

Example Single-Step Photobleaching Trace and Histogram of Alexa 546 Intensities

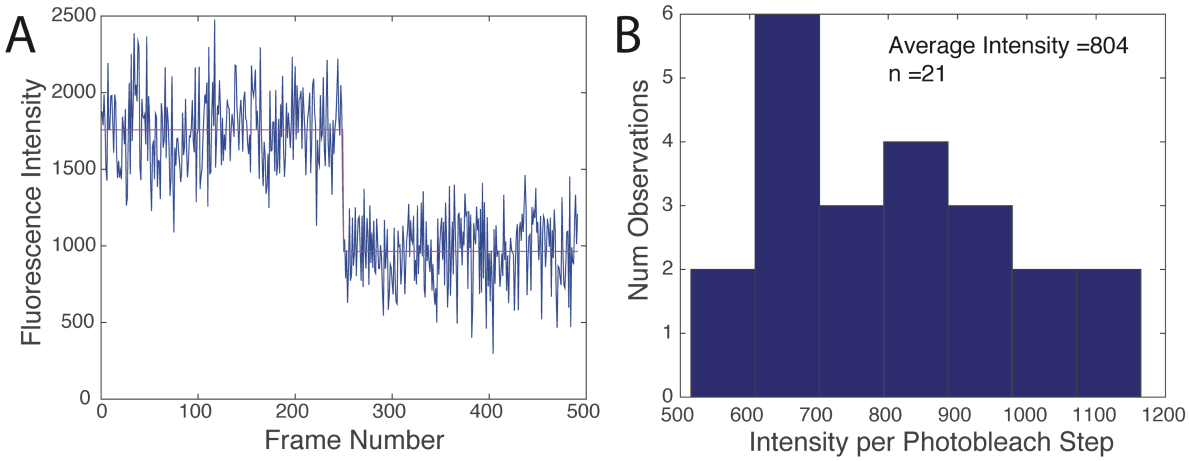

Figure S6. *(A) Example single-step photobleaching trace of an Alexa 546-labeled DNA-lipid inserted into a X-31 influenza virion, non-specifically bound to a glass coverslip. Red line shows the calculated step intensities, determined by a change point algorithm (see Image Analysis Details in Supporting Methods). (B) Histogram of fluorescence intensity per Alexa 546 photobleaching step obtained from the analysis of single-step photobleaching traces such as (A).*

Influence of GD1a Concentration in Target Vesicles on Viral Lipid Mixing Kinetics

To examine whether the concentration of GD1a in our target DNA-tethered vesicles influenced the influenza virus lipid mixing kinetics, we performed a single virus lipid mixing assay in which the virions were bound to target vesicles by GD1a receptor binding, and the target vesicles contained either 1% or 2% GD1a. We observed that the lipid mixing kinetics were identical within experimental error (see Figure S7), indicating that GD1a concentration across this range does not alter the viral lipid mixing kinetics.

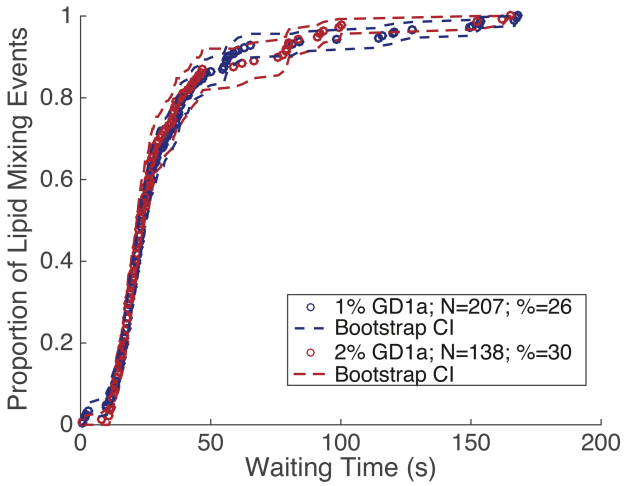

Figure S7*. Varying the GD1a concentration in the target vesicle twofold does not substantially alter the lipid mixing kinetics. CDFs of lipid-mixing waiting time distributions for single-virus*

fusion events are shown, together with bootstrap re-sampling error estimates (95% Confidence Intervals).

Movie Caption

Movie S1. *Example fluorescent video micrograph (Texas Red channel) showing several lipid mixing events between Texas Red-labeled influenza virus particles and DNA-tethered vesicles. Lipid-mixing events are identified as rapid increases in fluorescence, due to fluorescence de-quenching of Texas Red-DHPE upon lipid mixing with the target vesicle. The movie is sped up ~17x to aid in visualization (the actual data acquisition speed was 288 ms/frame). This is the same field of view as shown in Figure 5A.*

Supporting References

1. Van Lengerich, B., R.J. Rawle, P.M. Bendix, and S.G. Boxer. 2013. Individual vesicle fusion events mediated by lipid-anchored DNA. Biophys. J. 105: 409–419.

2. Domanska, M.K., R.A. Dunning, K.A. Dryden, K.E. Zawada, M. Yeager, and P.M. Kasson. 2015. Hemagglutinin Spatial Distribution Shifts in Response to Cholesterol in the Influenza Viral Envelope. Biophysical Journal. 109: 1917–1924.

3. Hutchinson, E.C., P.D. Charles, S.S. Hester, B. Thomas, D. Trudgian, M. Martínez-Alonso, and E. Fodor. 2014. Conserved and host-specific features of influenza virion architecture. Nature Communications. 5: 4816.

4. Shrirao, A.B., A. Hussain, C.H. Cho, and R. Perez-Castillejos. 2012. Adhesive-tape soft lithography for patterning mammalian cells: application to wound-healing assays. BioTechniques. 53: 315–318.

5. Chung, M., R.D. Lowe, Y.-H.M. Chan, P.V. Ganesan, and S.G. Boxer. 2009. DNA-tethered membranes formed by giant vesicle rupture. Journal of Structural Biology. 168: 190–199.

6. Pähler, G., C. Panse, U. Diederichsen, and A. Janshoff. 2012. Coiled-Coil Formation on Lipid Bilayers—Implications for Docking and Fusion Efficiency. Biophysical Journal. 103: 2295–2303.